electronics

MDPI

Article

Low-Voltage Low-Power Filters with Independent ω_0 and Q Tuning for Electronic Cochlea Applications

Waldemar Jendernalik *, Jacek Jakusz and Grzegorz Blakiewicz

Faculty of Electronics Telecommunications and Informatics, Gdańsk University of Technology, 80-233 Gdańsk, Poland; jacek.jakusz@pg.edu.pl (J.J.); grzegorz.blakiewicz@pg.edu.pl (G.B.)
* Correspondence: waldemar.jendernalik@pg.edu.pl

Abstract: An acoustic second-order low-pass filter is proposed for filter banks emulating the operation of a human cochlea. By using a special filter structure and an innovative quality (Q)-factor tuning technique, an independent change of the cutoff frequency (ω_0) and the Q-factor with unchanged gain at low frequencies is achieved in this filter. The techniques applied result in a simple filter design with low Q-factor sensitivity to component mismatch. These filter features greatly simplify the implementation of the electronic cochlea in CMOS technologies. An exemplary filter bank designed and simulated in an X-FAB 180 nm CMOS process is presented, which consumes 1.25–34.75 nW of power per individual filter when supplied with 0.5 V. The 11-channel filter bank covers a 20–20 kHz band, while the Q-factor of each channel can be tuned from 2 to 40. The simulation-predicted sensitivities of Q and ω_0 to process/voltage/temperature (PVT) variations are less than 1%. The input-referred noise is no greater than 22 μV_{RMS}, and the dynamic range is at least 68 dB for all filters in the bank.

Keywords: analog filters; low-frequency filters; audio filters; low-power circuits; analog integrated circuits; CMOS analog circuits; electronic cochlea

Citation: Jendernalik, W.; Jakusz, J.; Blakiewicz, G. Low-Voltage Low-Power Filters with Independent ω_0 and Q Tuning for Electronic Cochlea Applications. *Electronics* **2022**, *11*, 534. https://doi.org/10.3390/electronics11040534

Academic Editor: Daniel Dzahini

Received: 4 January 2022
Accepted: 9 February 2022
Published: 10 February 2022

1. Introduction

Systems for effective human speech processing and recognition are of increasing practical importance. They are used in controlling machines with the human voice [1], as well as in hearing aids [2–6]. Electronic circuits that emulate the operation of a human cochlea are gaining interest in such applications. The popularity of this approach comes from the belief that millions of years of evolution have led to a solution that is optimally suited for processing human speech in typical human environments. Work conducted on the physiology of hearing, particularly on the functioning of the cochlea, has enabled understanding the operation of this very important organ of the inner ear [7–9]. Due to the special properties of the cochlea, humans are able to hear and understand quiet speech even in environments with disruptive sounds. This highly desirable feature of human hearing is related to the ability of the cochlea to analyze and dynamically adjust to the properties of the sound heard. The cochlea processes the pressure of the received acoustic wave in multiple paths. Thus, the operation of the cochlea is similar to the operation of a system with multiple bandpass channels whose sensitivity is dynamically tuned to the volume of the sound, whereas out-of-band frequency components are largely suppressed. An accurate, complex model of the cochlea [10,11] takes into account both the processing of acoustic signals in individual ~~pass-band~~ channels and the coupling between the channels. However, due to practical limitations in electronic VLSI (very-large-scale integration) cochlea implementations, filter banks emulating only bandpass channels without coupling are most often used as compromise solutions [12–18]. Two architectures of the filter banks are used, consisting of elementary sections connected in cascade [12–15] or in parallel [16–18]. In both architectures, the key and difficult-to-implement feature

is the low-pass biquadratic filter section with electronically programmable cutoff frequency and quality factor. For precise signal processing, the frequency characteristics of biquadratic sections should be insensitive to process/voltage/temperature (PVT) variations.

A number of publications have been devoted to the design of filters intended for electronic cochlea. The earliest developed solutions [10–14] feature relatively high power consumption and supply voltage; therefore, they cannot be used in implants or systems with limited power supply (powered by small batteries). In addition, some of these solutions [12,13] do not provide sufficient accuracy in signal processing, which is limited by the influence of circuit parameter variations.

This paper proposes a new filter solution well suited to the requirements of an electronic cochlea powered by a small battery or small renewable energy source based on, e.g., thermoelectric generators or electromagnetic energy harvesters. By using a "transistorized" filter structure with transistors operating in the sub-threshold range [19], a significant reduction in voltage and power supply was achieved. As a result of the special tuning method of the filter quality factor and other applied techniques, a high robustness to PVT variations was obtained.

2. Proposed Filter Solution

2.1. Principle of Operation

The transfer function of the second-order low-pass filter (biquadratic) expressed in the Laplace domain is as follows:

$$H(s) = \frac{V_{out}(s)}{V_{in}(s)} = A \cdot \frac{\omega_0^2}{s^2 + s\omega_0 / Q_{LP} + \omega_0^2} \quad (1)$$

where V_{out} and V_{in} are the output and input voltages of the filter, A in V/V is the gain of the filter at zero frequency (DC gain), ω_0 in rad/s is the natural frequency ($\omega_0 = 2\pi f_0$), and Q_{LP} (dimensionless) denotes a quality factor.

Figure 1 shows a family of plots of the amplitude characteristics, $|H(j\omega)|$ versus ω, for three exemplary values of Q_{LP}. The plots are normalized for ω_0 of 1 rad/s, and A is assumed to be 1 V/V.

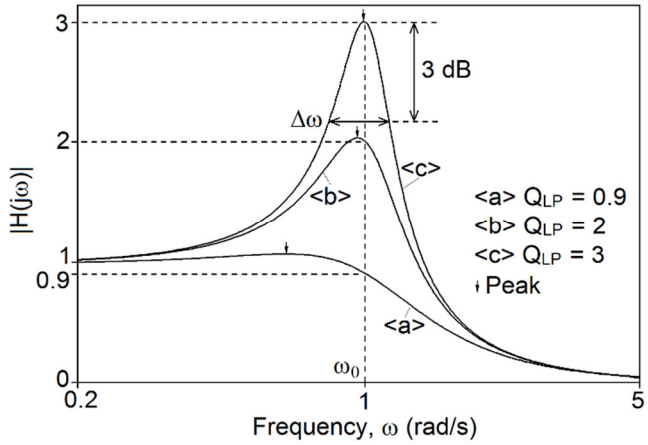

Q_{LP}	ω_0	$\lvert H(j\omega_0)\rvert$	ω_{peak}	$\lvert H(j\omega_{peak})\rvert$	ω_{L3dB}	ω_{H3dB}	Q_{BP}
0.9	1	0.9	0.620	1.08	—	1.143	—
1	1	1	0.707	1.15	—	1.170	—
2	1	2	0.934	2.06	0.624	1.165	1.72
3	1	3	0.972	3.04	0.784	1.128	2.82
4	1	4	0.984	4.03	0.849	1.104	3.86
5	1	5	0.990	5.02	0.883	1.085	4.90
6	1	6	0.993	6.02	0.905	1.073	5.91
7	1	7	0.994	7.02	0.920	1.064	6.90

$$Q_{BP} = \frac{\omega_{peak}}{\Delta\omega} \qquad \Delta\omega = \omega_{H3dB} - \omega_{L3dB}$$

Figure 1. A family of plots of the amplitude characteristics for different Q_{LP} (A = 1) and detailed numerical data on the plot parameters.

The bulged portion of the characteristic around ω_0 can be used for bandpass filtering if Q_{LP} is at least 2. In this case ($Q_{LP} \geq 2$), ω_0 and Q_{LP} can be treated as a center (or peak-gain) frequency and as a quality factor of a bandpass filter, i.e., ω_{center} (or ω_{peak}) and Q_{BP}. The detailed numerical data show that ω_0 is practically equal to ω_{peak} ($\omega_0 \cong \omega_{peak}$) if Q_{LP} is at least

2. The factor Q_{BP} is approximately equal to Q_{LP} ($Q_{BP} \approx Q_{LP}$) when Q_{LP} is 2–4, and Q_{BP} is practically equal to Q_{LP} ($Q_{BP} \cong Q_{LP}$) if Q_{LP} is 5 or more.

This particular shape of the characteristics allows this filter to emulate the basic properties of the cochlea in the human ear. By using an appropriate set of such filters, the functioning of the human inner ear can be imitated faithfully enough [12–18]. Electronic emulation of the cochlea uses filter banks in which each filter emulates particular resonant property of this organ. In simple terms, adaptation of the electronic cochlea to different sound levels involves splitting the sound spectrum into a number of channels with different center (peak-gain) frequencies, and then adjusting the gain in each channel individually. In channels where the sound strength is low, the filter gain is increased, and, in channels where the sound strength is high, the gain is reduced accordingly to achieve the most effective sound processing. To faithfully represent the physiological properties of the cochlea, the gain in the passband of each filter must be adjusted to mimic the ear's ability to adapt to different sound levels. This capability can be achieved by tuning the quality factor Q_{LP} of the low-pass filter since the value of this factor determines the value of the filter peak gain, as shown in Figure 1 ($|H(j\omega_{peak})| \approx Q_{LP}$ for $Q_{LP} < 2$, $|H(j\omega_{peak})| \cong Q_{LP}$ for $Q_{LP} \geq 2$).

Figure 2 shows a proposed filter that has the desirable feature of tuning the Q_{LP}-factor by changing the attenuation (k_Q). The filter consists of two transconductance amplifiers (G_{m1}, G_{m2}), two capacitors (C_1, C_2), and one attenuator (k_Q).

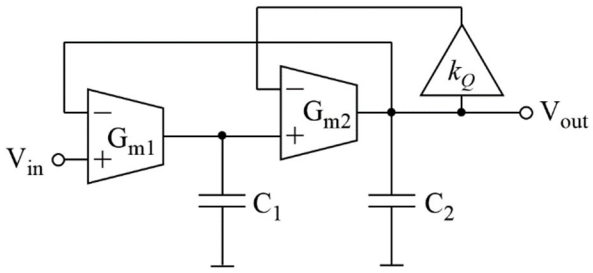

Figure 2. Proposed second-order low-pass filter with independent Q_{LP}-factor tuning (OTA-C structure).

The filter in Figure 2 has the transmittance in Equation (1), in which A, ω_0 and Q_{LP} are

$$A = 1, \quad \omega_0 = \sqrt{\frac{G_{m1}G_{m2}}{C_1C_2}}, \quad Q_{LP} = \frac{1}{k_Q} \cdot \sqrt{\frac{G_{m1}C_2}{G_{m2}C_1}} \tag{2}$$

where k_Q is the voltage gain (in V/V) of the attenuator. Thus, k_Q is assumed to be smaller than 1. All the undefined parameters have their usual meaning. The proposed high-Q filter structure with tunable Q is an extended version of the low-Q and not tunable structure presented in [19].

2.2. Sensitivity

In electronic cochlea emulators, banks consisting of many filters with center (peak-gain) frequencies of little difference are often used. In such solutions, it is particularly important to ensure that the peak gain frequencies and the peak gain magnitudes of the individual filters are sufficiently precise. The accuracy of filters implemented in CMOS technologies is influenced by the PVT variations. For the proposed filter in Figure 2, the influence of these factors on the peak gain frequency ($\cong\omega_0$) and the peak gain magnitude ($\cong Q_{LP}$) can be determined according to the following sensitivities:

$$\left|S_{k_{G12}}^{\omega_0}\right| = \left|\frac{d\omega_0/\omega_0}{dk_{G12}/k_{G12}}\right| = 0.5, \quad \left|S_{k_{C21}}^{\omega_0}\right| = 0.5, \quad S_{k_Q}^{\omega_0} = 0, \tag{3}$$

$$S_{k_{G12}}^{Q_{LP}} = \frac{dQ_{LP}/Q_{LP}}{dk_{G12}/k_{G12}} = 0.5, \quad S_{k_{C21}}^{Q_{LP}} = 0.5, \quad S_{k_Q}^{Q_{LP}} = -1, \tag{4}$$

where $G_{m1}/G_{m2} = k_{G12}$, and $C_2/C_1 = k_{C21}$.

While determining the sensitivities, the peak gain frequency ω_0 is assumed to be tuned by a simultaneous change of the transconductances G_{m1}, G_{m2} or capacitances C_1, C_2 such that their ratio G_{m1}/G_{m2} (or C_2/C_1) is constant and, thus, Q_{LP} remains unchanged. However, because of technology nonidealities, these ratios may vary, especially if an ω_0 tuning range is wide. Notice that the sensitivities in Equations (3) and (4) are relatively small (≤1) and do not depend on the value of Q_{LP}. This means that the inaccuracy of ω_0 and Q_{LP} does not exceed the inaccuracy of the parameters of the technology itself, which is a very advantageous feature of this filter structure. For example, a 1% variation in the transconductance ratio k_{G12} due to a technology imperfection induces only a 0.5% change in peak gain magnitude. Moreover, a high value of the peak gain magnitude can be obtained at low values of the transconductance and capacitance ratios, e.g., with k_{G12} and k_{C21} in the range of 1–2. Due to this, transconductors and capacitors of similar parameter values (unit components) can be used in the filter, which allows for an even better matching of these components, thereby obtaining a much better accuracy of ω_0 and Q_{LP} realization. In addition, the use of the unit components significantly simplifies the filter design.

2.3. Noise

The filter noise performance can be analyzed according to the schematic in Figure 3, in which the equivalent (input-referred) noise sources for each amplifier are introduced.

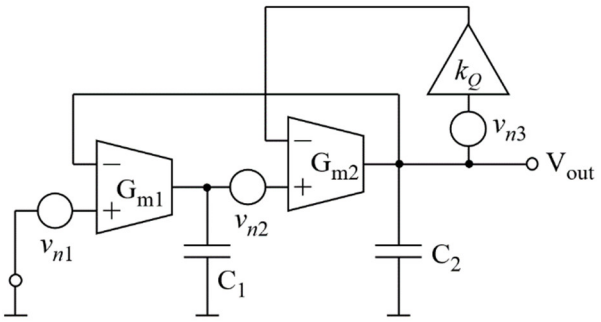

Figure 3. Schematic for noise analysis.

Assuming that the noise sources are characterized by the power spectral densities, $v_{n1}^2(\omega)$, $v_{n2}^2(\omega)$, and $v_{n3}^2(\omega)$, the respective powers of noise at the filter output are

$$v_{n1,out}^2(\omega) = v_{n1}^2(\omega)\cdot|H(j\omega)|^2, \quad v_{n2,out}^2(\omega) = v_{n2}^2(\omega)\cdot\left|\frac{j\omega C_1}{G_{m1}}\right|^2\cdot|H(j\omega)|^2,$$
$$v_{n3,out}^2(\omega) = v_{n3}^2(\omega)\cdot\left|\frac{-j\omega C_1 k_Q}{G_{m1}}\right|^2\cdot|H(j\omega)|^2. \tag{5}$$

Thus, the total noise power spectral density, referred to the filter input, is

$$v_{n,in}^2(\omega) = \frac{v_{n1,out}^2(\omega)+v_{n2,out}^2(\omega)+v_{n3,out}^2(\omega)}{|H(j\omega)|^2} = v_{n1}^2(\omega)+v_{n2}^2(\omega)\cdot\left(\frac{\omega C_1}{G_{m1}}\right)^2+v_{n3}^2(\omega)\cdot\left(\frac{\omega C_1}{G_{m1}}\right)^2\cdot k_Q^2. \tag{6}$$

It can be deduced from Equation (5) that the noise sources of the second transconductance amplifier and the voltage attenuator, v_{n2} and v_{n3}, are shaped identically due to the same factor of $\omega C_1/G_{m1}$. However, the attenuator's noise is reduced further due

to the factor of k_Q (k_Q is smaller than 1). As a result, the attenuator does not substantially degrade the filter noise performance.

2.4. Transistor-Level Circuit

The transistor-level implementation of the OTA-C structure of Figure 2 is shown in Figure 4. The operational transconductance amplifiers (OTAs) are composed of the transistors M_1–M_4 and 2×M_0. The additional transistors M_{SH1}, M_{SH2} are DC voltage shifters which improve the operating point conditions for OTAs [19]. All the transistors operate in the saturated subthreshold (weak inversion) region. The transconductances of OTAs are assumed to be identical, i.e., $G_{m1} = G_{m2} = I_\omega/(n_p \cdot U_T)$ (n_p is the subthreshold slope factor for p-channel transistors, U_T is the thermal voltage, $U_T = k \cdot T/q$). The filter capacitances are also assumed to be identical, $C_1 = C_2$. By using the floating capacitors ($C_1/2$, $C_2/2$), a twofold reduction in total capacitance and, thus, the area occupied by the filter was achieved [19].

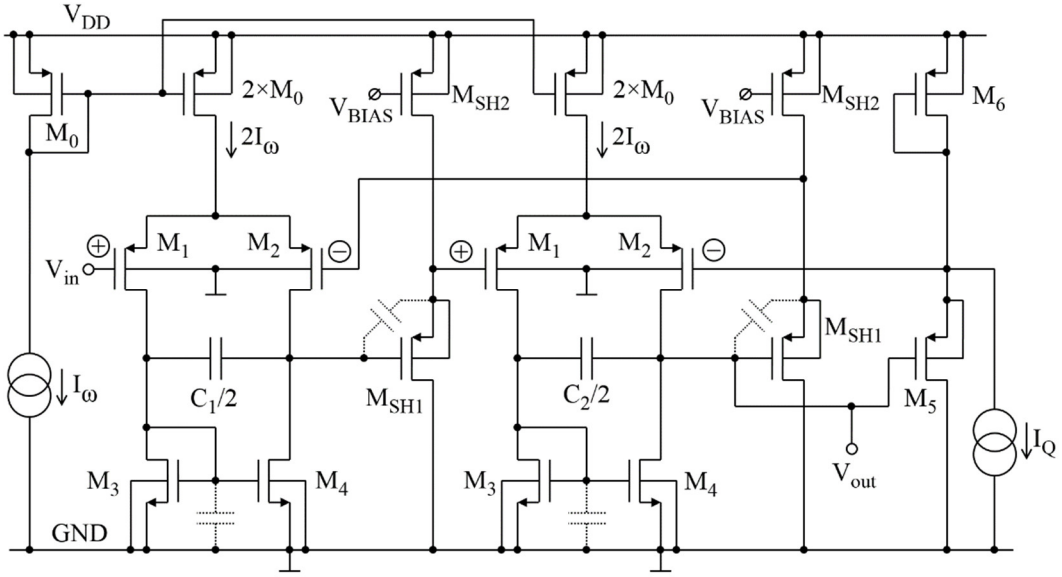

Figure 4. Transistor-level implementation of the filter in Figure 2.

The attenuator consists of transistors M_5–M_6 and the current source I_Q. Its gain depends on the transconductance of the transistors M_5 and M_6, i.e., $k_Q = g_{m5}/(g_{m5} + g_{m6})$. For I_Q equal to zero, both transistors M_5 and M_6 conduct the same current; therefore, $g_{m6} = g_{m5}$, and $k_Q = 1/2$. Increasing I_Q makes the current flowing through M_6 larger than that through M_5; as a result, k_Q decreases, according to the following formula:

$$k_Q = \frac{1}{2}\left(1 - \frac{1}{\sqrt{1 + 4I_q^2/I_Q^2}}\right) \approx \frac{1}{2}\left(1 - \frac{I_Q}{2I_q}\right) \tag{7}$$

where I_q is a quiescent (DC) current flowing through M_5 and M_6 when I_Q is zero.

For the filter in Figure 4, the transmittance parameters can be tuned independently by the currents I_ω and I_Q, as explained by Equation (7) and the following formulas:

$$A = 1, \quad \omega_0 = \sqrt{\frac{G_{m1}G_{m2}}{C_1C_2}} = \frac{I_\omega}{n_pU_T} \cdot \frac{1}{\sqrt{C_1C_2}}, \quad Q_{LP} = \frac{1}{k_Q} \cdot \sqrt{\frac{G_{m1}C_2}{G_{m2}C_1}} = \frac{1}{k_Q} \tag{8}$$

where $G_{m1} = G_{m2}$, $C_1 = C_2$, and $k_Q \le 1/2$ are assumed.

For the assumed $k_Q \le 1/2$ ($Q_{LP} \ge 2$), ω_0 is practically equal to ω_{peak}, while Q_{LP} is well correlated with the peak gain magnitude and Q_{BP}, as explained in Section 2.1; thus, the designed filter satisfies the following equations:

$$A = 1, \quad \omega_{peak} \cong \omega_0, \quad \text{peak gain} \cong 1/k_Q, \quad Q_{BP} \approx 1/k_Q. \tag{9}$$

3. Filter Bank

An exemplary set of 11 filters was designed to cover the full audio band from 20 Hz to 20 kHz. Thus, the peak-gain frequencies f_{peak} ($f_{peak} = \omega_{peak}/2/\pi$) of the consecutive filters form an octave series, i.e., 20, 40, 80, …, 10240, and 20480 Hz. The transistor sizes (in μm/μm) in all filters are M_0 = 10/6, $M_1 = M_2$ = 8/2, $M_3 = M_4$ = 10/10, $M_5 = M_6$ = 2/2, M_{SH1} = 30/3, M_{SH2} = 10/6. The bias current flowing through transistors M_{SH1}–M_{SH2} is 0.25 nA. The values of the current setting the filter frequencies and the capacitances used in each filter are specified in Table 1.

Table 1. Simulated [1] post-layout parameters of the individual filters with V_{DD} = 0.5 V.

Target f_{peak} (Hz)	**20**	**40**	**80**	**160**	**320**	**640**	**1280**	**2560**	**5120**	**10,240**	**20,480**
I_ω (nA)	0.5	0.5	1	1	2	2	4	4	8	16	16
$C_1/2$, $C_2/2$ (pF) [2]	62.36	31.13	30.54	15.22	14.81	7.35	7.09	3.49	3.34	3.16	1.53
Power (nW) [3]	1.25–3.75	1.25–3.75	2.25–4.75	2.25–4.75	4.25–6.75	4.25–6.75	8.25–10.75	8.25–10.75	16.25–18.75	32.25–34.75	32.25–34.75
Obtained f_{peak} (Hz) [3]	18.52–19.88	38.16–40.95	74.67–80.47	157.15–159.7	298.2–319.4	595.5–639.3	1192–1276	2399–2568	4801–5121	9547–10230	19050–20450

[1] CMOS process: X-FAB xh018. Transistors: 1.8 V, low-VT MOSFETs. Device models: nominal. [2] Single-density (1 fF/μm²) MIM capacitor values after taking layout parasitics into account. [3] For k_Q tuned from 1/2 to 1/100 (I_Q tuned within 0–5 nA).

Figure 5 presents the amplitude characteristics of the filter bank for different values of parameter k_Q, i.e., for different target peak gain values. The gain nonuniformity of the filter bank is relatively small, with differences between the peak gains of individual filters of ±0.5 dB for low gains and ±1 dB for high gains. The DC gain is 0 dB in all filters (A = 1). Note also that all filters feature a high stop-band attenuation of at least 50 dB.

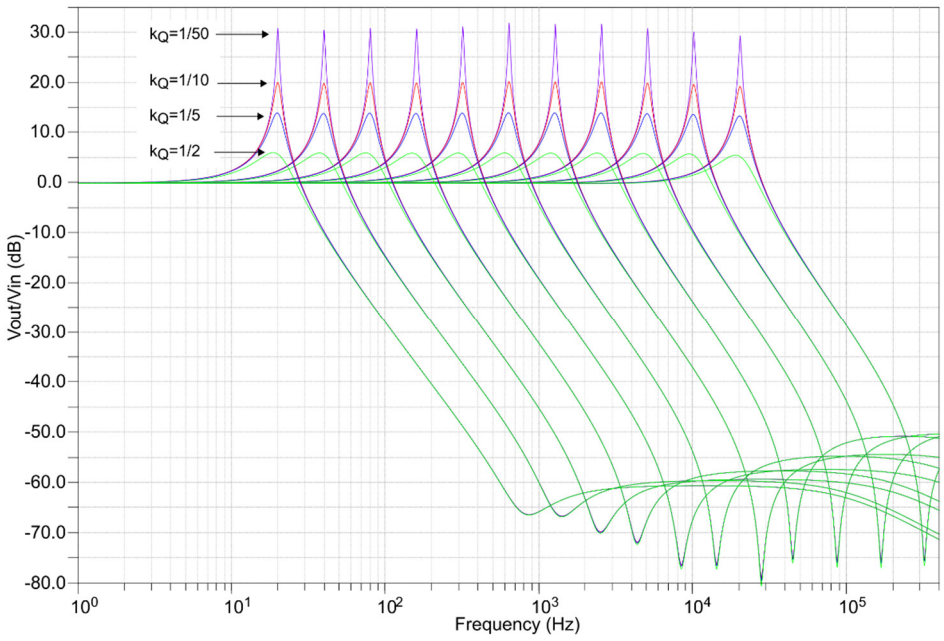

Figure 5. Amplitude responses of the filter bank simulated using nominal device models.

The detailed values of the obtained peak gain magnitude, peak gain frequency f_{peak}, and values of the factor Q_{BP} are in Figure 6a–c. These figures show zoomed-in passband portions of the amplitude characteristics for the three selected filters: for the lowest (20 Hz), middle (1.28 kHz), and highest (20.48 kHz) frequencies, respectively.

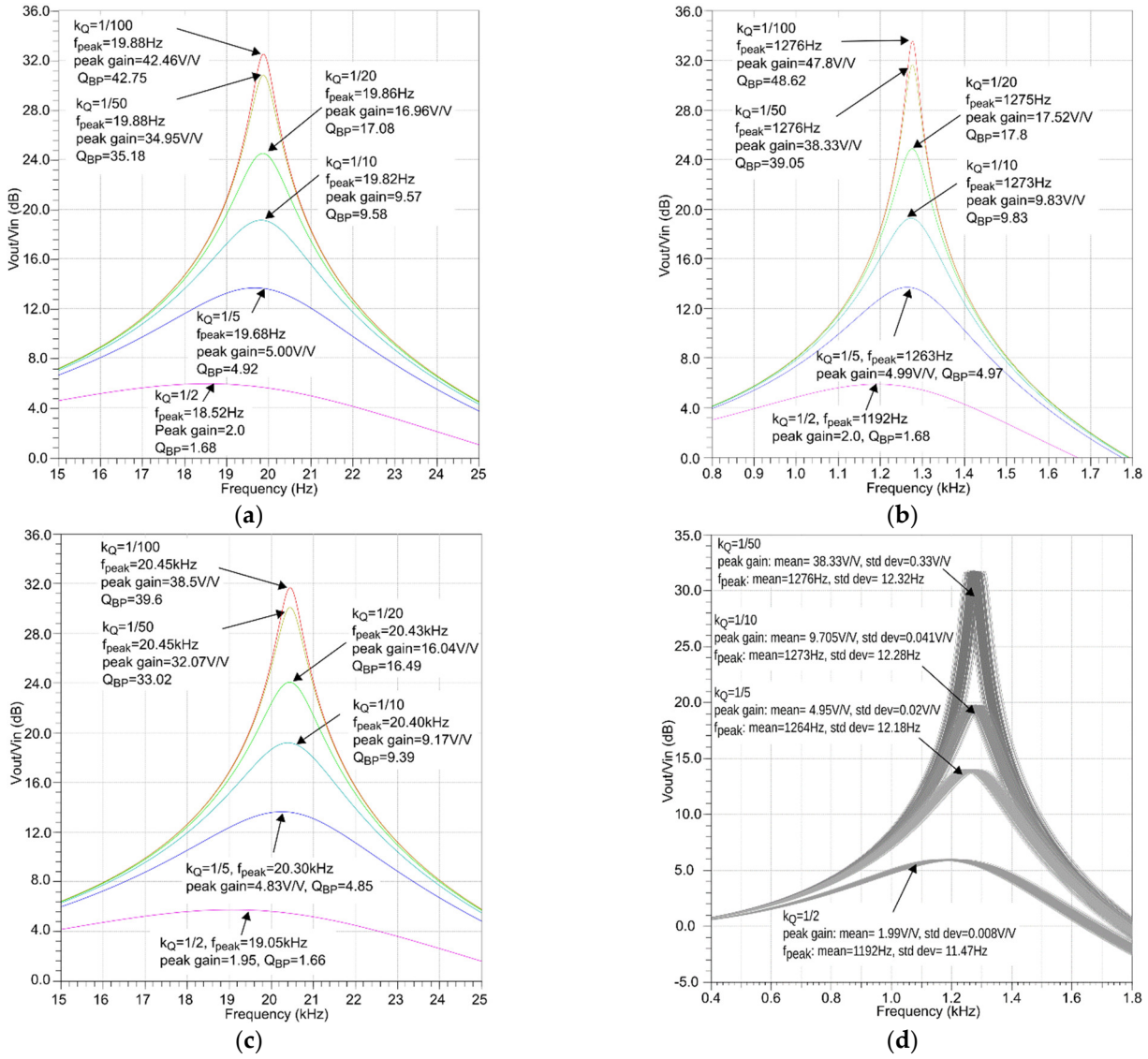

Figure 6. Simulated amplitude responses of the selected filters: (**a–c**) 20 Hz, 1.28 kHz, and 20.48 kHz filters (nominal simulation); (**d**) 1.28 kHz filter under technology mismatch (500 Monte Carlo simulation runs).

In Figure 6a–c, it can be seen that, for small and medium values, the peak gain of the filters is approximately equal to Q_{BP} ($Q_{BP} \approx$ peak gain), which is consistent with the theory illustrated in Figure 1. However, at large values of the peak gain, the Q tuning process becomes nonlinear, i.e., the peak gain is no longer directly proportional to $1/k_Q$ as shown in Equation (9). For example, in Figure 6b, the peak gain is 17.5 V/V for k_Q of 1/20 V/V, and the peak gain is 38 when k_Q is 1/50. This is caused by finite output resistance of OTAs (0.3–1.5 GΩ) which limits the maximum peak gain to 50–55 V/V. The tuning of the peak gain frequency is performed according to Equation (9), i.e., $\omega_{peak} \cong \omega_0$. The results in Figure 6a–c show that, when the quality factor increases, ω_{peak} (f_{peak}) moves from left to right, approaching the target value of ω_0 (f_0) (which is consistent with the theory in Figure 1). Details of the obtained f_{peak} values are also given in Table 1.

Simulations which take into account technology parameter variation and component mismatch show that the peak-gain-magnitude and peak-gain-frequency variations are less than 1% (1 sigma) for all filters in the bank. Exemplary Monte Carlo simulation results for the middle-band 1.28-kHz filter are shown in Figure 6d. Details of this filter's performance under PVT variations are provided in the Appendix A.

All the filters feature a maximum amplitude of the input sinusoidal signal of at least 86 mV_{peak} at 1% output THD (fundamental frequency = $f_0/10$). The input-referred noise integrated from 1 Hz to $2f_0$ is less than 22 μV_{RMS} for all the filters, resulting in a filter bank dynamic range of 68 dB.

4. Discussion

The filter shown in Figure 7 is often used in many practical implementations of an electronic cochlea [12–15,20]. Therefore, this section compares the key features of this filter, which has become the preferred solution in the cochlea, with the features of the proposed new filter structure shown in Figure 2.

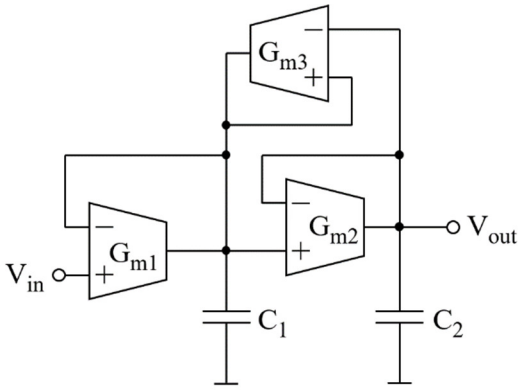

Figure 7. Structure of a second-order low-pass filter frequently used in electronic cochlea implementations.

The filter in Figure 7 has the transmittance in Equation (1) with the following parameters:

$$A = 1, \quad \omega_0 = \sqrt{\frac{G_{m1}G_{m2}}{C_1C_2}}, \quad Q_{LP} = \left[\frac{C_2}{C_1}\left(\frac{G_{m1}}{G_{m2}} - \frac{G_{m3}}{G_{m2}}\right) + 1\right]^{-1} \cdot \sqrt{\frac{G_{m1}C_2}{G_{m2}C_1}} \tag{10}$$

The frequency ω_0 can be tuned in the same manner as in the proposed filter, shown in Figure 2, by changing G_{m1}, G_{m2} or C_1, C_2. To achieve ω_0 tuning independent of Q_{LP}, it is necessary to keep constant values of the transconductance G_{m1}/G_{m2} and capacitance C_1/C_2 ratios. Under these conditions, Q_{LP} tuning requires changing the transconductance of the positive-feedback-connected amplifier (G_{m3}). With these assumptions, the sensitivities of Q_{LP} to variations in transconductance and capacitance ratios are

$$S_{k_{G12}}^{Q_{LP}} = \frac{1}{2} - \sqrt{k_{G12}k_{C21}} \cdot Q_{LP}, \quad S_{k_{C21}}^{Q_{LP}} = \frac{1}{2} - \sqrt{\frac{k_{C21}}{k_{G12}}} \cdot (k_{G12} - k_{G32}) \cdot Q_{LP}, \quad S_{k_{G32}}^{Q_{LP}} = \sqrt{\frac{k_{C21}}{k_{G12}}} \cdot k_{G32} \cdot Q_{LP}, \tag{11}$$

where k_{G12} and k_{C21} are defined in Equation (4), and $k_{G32} = G_{m3}/G_{m2}$.

For a practical design case, i.e., $k_{G12} = k_{C21} = 1$, the quality factor is $Q_{LP} = 1/(2-k_{G32})$, and Equation (10) becomes

$$S_{k_{G12}}^{Q_{LP}} = \frac{1}{2} - Q_{LP}, \quad S_{k_{C21}}^{Q_{LP}} = -\left(\frac{1}{2} - Q_{LP}\right), \quad S_{k_{G32}}^{Q_{LP}} = 2Q_{LP} - 1. \tag{12}$$

Comparing Equations (3) and (11), defining the sensitivities of the compared filters, it can be observed that, for all practical cases when $Q_{LP} \geq 2$, the proposed filter has a much

lower sensitivity to implementation mismatch between the transconductors (G_{m1}, G_{m2}) and the capacitors (C_1, C_2). Thus, the proposed filter is better suited for practical implementation in CMOS technologies.

5. Comparison to the State of the Art and Conclusions

Requirements for the filter banks used in electronic cochlea implementation depend on their application. In systems designed to control machines with the human voice, the values of the supply voltage and power consumption are usually less important, whereas the precision of the frequency characteristics is crucial. The most difficult criteria to meet are those related to hearing aid implants and devices for Internet of things. In such cases, low supply voltage and low power consumption must additionally be ensured due to the fact that such devices are powered from small batteries or small renewable energy sources based on, e.g., thermoelectric generators or electromagnetic energy harvesters. Therefore, in the presented comparison of the filter banks reported in the literature (Table 2), special attention was paid to these critical parameters.

Table 2. Performance comparison of filter banks designed for electronic cochlea.

Parameter	This Work (Simulated)	[15] (Measured)	[16] (Measured)	[17] (Measured)	[18] (Measured)
Technology	0.18 µm CMOS	0.35 µm CMOS	0.35 µm CMOS	1.5 µm BiCMOS	0.18 µm CMOS
Channel count	11	64×2	1	16	64 × 2
Supply voltage	0.5 V	3.3 V	3.3 V	2.8 V	0.5 V
Power consumption per single filter	1.25–34.75 nW	NA	13–20 µW [1]	112 nW–5.4 µW	0.13–100 nW [2]
Filter type	OTA-C	OTA-C	Floating active inductors	OTA-C	Source follower based
Signal-to-noise ratio	68 dB @1% THD	36 dB 52 dB [3]	17–27 dB for HQ 24–32 dB for LQ [4] @5% THD	57 dB IDR [5]	40 dB for $Q \approx 10$ 55 dB for $Q \approx 1$ @1% HD
f_0 tuning range	20 Hz–20 kHz	100 Hz–20 kHz	31 Hz–8 kHz	200 Hz–6 kHz	8 Hz–20 kHz
f_0 matching (1σ)	±1%	±6%	NA	NA	±3.3%
Q tuning range	2–40	NA	2–19	1–10	1.3–39
Q matching (1σ)	±1%	±27% for $Q = 1.5$	NA	NA	±15%

[1] Estimated value. [2] Estimated without a programmable gain amplifier. [3] With preamp gain control. [4] HQ—high quality factors, LQ—low quality factors. [5] IDR—internal dynamic range.

In the proposed filter bank, similarly to the implementation in [18], a relatively low supply voltage of 0.5 V was used, which allowed a reduction in power consumption. Note that, in [18], an additional programmable gain amplifier was required for proper operation of the filter, whose power supply is not included in the data in Table 1. Having this fact in mind, it can be concluded that the proposed solution is more beneficial in terms of power consumption. In practical implementation of the filters in CMOS technology, an important problem is to obtain a low sensitivity of the center frequency f_0 and the quality (Q) factor to PVT variations. This issue is particularly important in systems with a large number of channels [15,17,18], where the center frequencies of consecutive channels do not differ much. For this reason, a special adjustment system is used in the implementation [15]. Such a solution complicates the whole system, increasing its area and power consumption. The data in Table 2 show that the variation of f_0 and Q in the proposed filter bank is smaller compared to the other solutions. Another very critical problem in the solution proposed in [18] is a quadratic dependence of the filter gain at low frequencies on

the *Q*-factor value. The consequence of such a dependence is a reduction in signal dynamics. This reduction results from the fact that, e.g., a fivefold increase in the filter *Q*-factor leads to a 25-fold increase in the filter gain and, consequently, the output signal amplitude. To reduce the impact of this phenomenon, additional attenuators at the filter input were applied in [18]. As can be seen from Equations (1) and (2), the proposed filter is free from this unfavorable feature because the low-frequency (DC) gain is always equal to one (A = 1).

Author Contributions: All authors contributed equally to conceptualization, methodology, formal analysis, simulations, writing—original draft preparation, and writing—review and editing. All authors have read and agreed to the published version of the manuscript.

Funding: This research was funded in part by the National Science Centre of Poland under grant 2016/23/B/ST7/03733.

Institutional Review Board Statement: Not applicable.

Informed Consent Statement: Not applicable.

Data Availability Statement: Not applicable.

Conflicts of Interest: The authors declare no conflicts of interest. The funders had no role in the design of the study; in the collection, analyses, or interpretation of data; in the writing of the manuscript, or in the decision to publish the results.

Appendix A

This appendix provides, in Tables A1, A2, and A3, simulation results of the proposed filter performance under PVT variations (process: CMOS X-FAB 180 nm xh018).

Table A1. Corner simulation results for the middle-band filter at V_{DD} of 0.5 V.

	T = 0 °C					T = 27 °C					T = 50 °C				
k_Q	TM	WP	WS	WO	WZ	TM	WP	WS	WO	WZ	TM	WP	WS	WO	WZ
								f_{peak} (Hz)							
1/50	1360	1395	1313	1326	1380	1281	1312	1246	1259	1298	1211	1241	1176	1187	1228
1/10	1357	1393	1309	1323	1378	1279	1310	1244	1256	1296	1208	1239	1173	1185	1226
1/5	1349	1385	1299	1312	1370	1271	1302	1235	1247	1288	1200	1231	1165	1177	1218
1/2	1274	1309	1221	1233	1295	1201	1231	1165	1177	1218	1134	1163	1099	1109	1152
								peak gain (V/V)							
1/50	43.47	69.35	18.34	18.08	68.44	70.29	79.3	43.9	43.59	77.25	76.53	53.82	66.47	66.69	51.48
1/10	10.13	11.11	7.658	7.62	11.04	11.11	11.35	10.11	10.11	11.24	11.24	10.65	10.93	10.95	10.49
1/5	5.15	5.4	4.421	4.41	5.367	5.39	5.456	5.137	5.14	5.413	5.42	5.296	5.325	5.34	5.238
1/2	2.03	2.067	1.907	1.91	2.055	2.06	2.076	2.023	2.03	2.061	2.07	2.056	2.047	2.05	2.039
								DC gain (V/V)							
1/50	0.9988	0.9992	0.998	0.9989	0.9956	0.9991	0.9999	0.9985	0.9996	0.9957	0.9997	1.003	0.9987	0.9999	0.9979
1/10	0.9979	0.9986	0.9961	0.9970	0.995	0.9984	0.9994	0.9976	0.9987	0.9951	0.9991	1.002	0.998	0.9992	0.9971
1/5	0.9968	0.9978	0.9938	0.9947	0.9942	0.9977	0.9986	0.9965	0.9976	0.9943	0.9983	1.001	0.9972	0.9984	0.996
1/2	0.9932	0.9953	0.9862	0.9871	0.9917	0.9951	0.9962	0.9929	0.9940	0.9919	0.9958	0.9974	0.9945	0.9957	0.9925

Table A2. Corner simulation results for the middle-band filter at V_{DD} of 0.475 V.

	T = 0 °C					T = 27 °C					T = 50 °C				
k_Q	TM	WP	WS	WO	WZ	TM	WP	WS	WO	WZ	TM	WP	WS	WO	WZ
								f_{peak} (Hz)							
1/50	1354	1392	1294	1307	1377	1279	1311	1243	1255	1297	1211	1241	1177	1189	1228
1/10	1351	1390	1289	1302	1375	1277	1309	1240	1252	1295	1209	1239	1174	1186	1226
1/5	1342	1381	1277	1290	1366	1269	1300	1231	1244	1287	1201	1231	1166	1178	1219
1/2	1266	1306	1194	1206	1291	1199	1230	1160	1171	1217	1135	1164	1100	1111	1152
								peak gain (V/V)							

1/50	32.3	58.25	11.35	11.15	57.58	58.79	72.47	32.57	32.22	70.68	69.53	53.11	54.71	54.61	50.81
1/10	9.364	10.78	6.081	6.03	10.69	10.77	11.19	9.356	9.34	11.06	11.08	10.62	10.56	10.58	10.44
1/5	4.945	5.318	3.842	3.83	5.275	5.311	5.419	4.933	4.94	5.363	5.38	5.288	5.238	5.25	5.216
1/2	1.996	2.055	1.792	1.79	2.039	2.052	2.07	1.991	1.99	2.05	2.061	2.055	2.035	2.04	2.031
DC gain (V/V)															
1/50	0.9984	0.9989	0.9967	0.9978	0.994	0.9987	0.9996	0.9980	0.9994	0.9937	0.9993	1.002	0.9982	0.9998	0.9955
1/10	0.9973	0.9982	0.9938	0.9949	0.9933	0.998	0.999	0.9969	0.9983	0.9931	0.9987	1.001	0.9975	0.9990	0.9946
1/5	0.9959	0.9974	0.9901	0.9911	0.9924	0.9971	0.9982	0.9955	0.9969	0.9923	0.9979	1	0.9966	0.9981	0.9936
1/2	0.9913	0.9945	0.9782	0.9792	0.9895	0.9942	0.9957	0.9910	0.9923	0.9897	0.9952	0.9969	0.9935	0.9950	0.9901

Table A3. Corner simulation results for the middle-band filter at V_{DD} of 0.525 V.

	T = 0 °C					**T = 27 °C**					**T = 50 °C**				
k_Q	**TM**	**WP**	**WS**	**WO**	**WZ**	**TM**	**WP**	**WS**	**WO**	**WZ**	**TM**	**WP**	**WS**	**WO**	**WZ**
f_{peak} (Hz)															
1/50	1364	1397	1323	1338	1383	1282	1313	1247	1260	1299	1209	1240	1172	1184	1227
1/10	1361	1395	1320	1335	1380	1279	1310	1245	1258	1297	1206	1238	1169	1181	1226
1/5	1353	1387	1311	1324	1372	1272	1302	1237	1249	1289	1199	1230	1161	1173	1218
1/2	1278	1312	1235	1248	1298	1202	1232	1167	1179	1219	1132	1162	1095	1106	1151
peak gain (V/V)															
1/50	55.63	79.94	27.41	27.11	78.8	81.4	84.94	56.47	56.28	82.8	82.45	53.81	78.38	78.87	51.44
1/10	10.68	11.36	8.897	8.87	11.3	11.36	11.46	10.66	10.67	11.37	11.35	10.65	11.18	11.21	10.51
1/5	5.294	5.459	4.81	4.81	5.433	5.451	5.483	5.273	5.28	5.448	5.441	5.296	5.381	5.39	5.247
1/2	2.051	2.076	1.974	1.98	2.067	2.072	2.08	2.043	2.05	2.069	2.069	2.057	2.053	2.06	2.043
DC gain (V/V)															
1/50	0.9991	0.9995	0.9986	0.9993	0.9968	0.9993	1	0.9988	0.9993	0.997	1	1.003	0.9990	1.0000	0.9997
1/10	0.9983	0.9989	0.9973	0.9980	0.9962	0.9988	0.9996	0.9981	0.9980	0.9965	0.9995	1.002	0.9985	0.9994	0.9988
1/5	0.9974	0.9982	0.9956	0.9964	0.9955	0.9981	0.9989	0.9972	0.9964	0.9958	0.9987	1.001	0.9977	0.9987	0.9977
1/2	0.9944	0.9958	0.9903	0.9911	0.9931	0.9957	0.9966	0.9942	0.9911	0.9934	0.9963	0.9978	0.9953	0.9962	0.9942

References

1. Russo, M.; Stella, M.; Sikora, M.; Pekić, V. Robust Cochlear-Model-Based Speech Recognition. *Computers* **2019**, *8*, 5. https://doi.org/10.3390/computers8010005.
2. Raychowdhury, A.; Tokunaga, C.; Beltman, W.; Deisher, M.; Tschanz, J.W.; De, V. A 2.3 nJ/frame voice activity detector-based audio front-end for context-aware system-on-chip applications in 32-nm CMOS. *IEEE J. Solid-State Circuits* **2013**, *48*, 1963–1969. https://doi.org/10.1109/JSSC.2013.2258827.
3. Price, M.; Glass, J.; Chandrakasan, A.P. A 6 mW, 5000-word real-time speech recognizer using WFST models. *IEEE J. Solid-State Circuits* **2015**, *50*, 102–112. https://doi.org/10.1109/JSSC.2014.2367818.
4. Yang, G.; Lyon, R.F.; Drakakis, E.M. A 6 μW per channel analog biomimetic cochlear implant processor filterbank architecture with across channels AGC. *IEEE Trans. Biomed. Circuits Syst.* **2015**, *9*, 72–86. https://doi.org/10.1109/TBCAS.2014.2325907.
5. Harczos, T.; Chilian A.; Husar. P. Making use of auditory models for better mimicking of normal hearing processes with cochlear implants: The SAM coding strategy. *IEEE Trans. Biomed. Circuits Syst.* **2013**, *7*, 414–425. https://doi.org/10.1109/TBCAS.2012.2219530.
6. Yip, M.; Jin, R.; Nakajima, H.H.; Stankovic, K.M.; Chandrakasan, A.P. A Fully-Implantable Cochlear Implant SoC With Piezoelectric Middle-Ear Sensor and Arbitrary Waveform Neural Stimulation. *IEEE J. Solid-State Circuits* **2015**, *50*, 214–229. https://doi.org/10.1109/JSSC.2014.2355822.
7. Robles, L.; Ruggero, M.A.; Rich, N.C. Mössbauer measurements of the mechanical response to single-tone and two-tone stimuli at the base of of the chinchilla cochlea. In *Peripheral Auditory Mechanisms;* Allen, J.B., Hall, J.L., Hubbard, A., Neely, S.T., Tubis, A., Eds.; Springer: Berlin/Heidelberg, Germany, 1986; pp. 121–128. https://doi.org/10.1007/978-3-642-50038-1_16.
8. Ruggero, M.A.; Narayan, S.S.; Temchin, A.N.; Recio, A. Mechanical bases of frequency tuning and neural excitation at the base of the cochlea: Comparison of basilar-membrane vibrations and auditory-nerve-fiber responses in chinchilla. *Proc. Natl. Acad. Sci. USA* **2000**, *97*, 11744–11750. https://doi.org/10.1073/pnas.97.22.11744.
9. Plack, C.J. *The Sense of Hearing*; Lawrence Erlbaum Associates: Mahwah, NJ, USA, 2005; ISBN 0805848843/9780805848847.
10. Hamilton, T.J.; Jin, C.; van Schaik, A.; Tapson, J. An active 2-D silicon cochlea. *IEEE Trans. Biomed. Circuits Syst.* **2008**, *2*, 30–43. https://doi.org/10.1109/TBCAS.2008.921602.

11. Wen, B.; Boahen, K. A silicon cochlea with active coupling. *IEEE Trans. Biomed. Circuits Syst.* **2009**, *3*, 444–455. https://doi.org/10.1109/TBCAS.2009.2027127.
12. Lyon, R.F.; Mead, C. An analog electronic cochlea. *IEEE Trans. Acoust., Speech Signal Process.* **1988**, *36*, 1119–1134. https://doi.org/10.1109/29.1639.
13. Watts, L.; Kerns, D.A.; Lyon, R.F.; Mead, C.A. Improved implementation of the silicon cochlea. *IEEE J. Solid-State Circuits* **1992**, *27*, 692–700. https://doi.org/10.1109/4.133156.
14. Sarpeshkar, R.; Lyon, R.F.; Mead, C.A. An analog VLSI cochlea with new transconductance amplifiers and nonlinear gain control. In Proceedings of the 1996 IEEE International Symposium on Circuits and Systems. Circuits and Systems Connecting the World. ISCAS 96, Atlanta, GA, USA, 15 May 1996; Volume 3, pp. 292–296. https://doi.org/10.1109/ISCAS.1996.541591.
15. Liu, S.-C.; van Schaik, A.; Minch, B.A.; Delbruck, T. Asynchronous binaural spatial audition sensor with 2 × 64 × 4 channel output. *IEEE Trans. Biomed. Circuits Syst.* **2014**, *8*, 453–464. https://doi.org/10.1109/TBCAS.2013.2281834.
16. Wang, S.; Koickal, T.J.; Hamilton, A.; Cheung, R.; Smith, L.S. A bio-realistic analog CMOS cochlea filter with high tunability and ultra-steep roll-off. *IEEE Trans. Biomed. Circuits Syst.* **2015**, *9*, 297–311. https://doi.org/10.1109/TBCAS.2014.2328321.
17. Sarpeshkar, R.; Salthouse, C.; Sit, J.-J.; Baker, M.W.; Zhak, S.M.; Lu, T.K.-T.; Turicchia, L.; Balster, S. An ultra-low-power programmable analog bionic ear processor. *IEEE Trans. Biomed. Eng.* **2005**, *52*, 711–727. https://doi.org/10.1109/TBME.2005.844043.
18. Yang, M.; Chien, C.-H.; Delbruck, T.; Liu, S.-C. A 0.5 V 55 μW 64 × 2 Channel Binaural Silicon Cochlea for Event-Driven Stereo-Audio Sensing. *IEEE J. Solid-State Circuits* **2016**, *51*, 2554–2569. https://doi.org/10.1109/JSSC.2016.2604285.
19. Jendernalik, W.; Jakusz, J.; Blakiewicz, G. Ladder-Based Synthesis and Design of Low-Frequency Buffer-Based CMOS Filters. *Electronics* **2021**, *10*, 2931–2943. https://doi.org/10.3390/electronics10232931.
20. Grech, I.; Micallef, J.; Azzopardi, G.; Debono, C.J. A 0.9 V wide-input-range bulk-input CMOS OTA for G_M-C filters. In Proceedings of the 10th IEEE International Conference on Electronics, Circuits and Systems, 2003. ICECS 2003. Proceedings of the 2003, Sharjah, United Arab Emirates, 14–17 December 2003; Volume 2, pp. 818–821. https://doi.org/10.1109/ICECS.2003.1301912.